

<https://doi.org/10.1038/s42005-024-01632-7>

# Alternative routes to electron hydrodynamics



Jorge Estrada-Álvarez , Francisco Domínguez-Adame &amp; Elena Díaz

Viscous flow of interacting electrons in two dimensional materials features a bunch of exotic effects. A model resembling the Navier–Stokes equation for classical fluids accounts for them in the so called hydrodynamic regime. We perform a detailed analysis of the physical conditions to achieve electron hydrodynamic transport and find alternative routes: the application of a magnetic field or a high-frequency electric field in the absence of very frequent inelastic collisions. As a major conclusion, we show that the conventional requirement of frequent electron–electron collisions is too restrictive and, as a consequence, materials and phenomena to be described using hydrodynamics are widened. In view of our results, we discuss recent experimental evidence on viscous flow and point out alternative avenues to reduce electric dissipation in optimized devices.

Viscous electron flow in two-dimensional (2D) materials is a collective motion of conduction electrons<sup>1–4</sup> that results in exotic phenomena such as curved current profiles<sup>5</sup>, the superballistic effect<sup>6</sup> and electron whirlpools<sup>7–9</sup>. Both the recent realization of these counterintuitive effects and the potential applications<sup>10,11</sup> in 2D devices have attracted the attention towards this field. The collective motion of electrons is fully characterized by macroscopic variables<sup>12</sup>, by using continuum models<sup>1,2,7,13,14</sup> similar to the Navier–Stokes equation (NSE) for ordinary fluids, hence the name of electron hydrodynamics. The conventional route towards viscous electron flow is favouring electron–electron collisions, also known as elastic scattering events since they conserve the total momentum of the system. The requirement reads as  $l_{ee} < W^{3,5}$  or, more strictly with the condition  $l_{ee} < l_e$  too<sup>1,2,7</sup>, where  $W$  is the size of the device,  $l_{ee}$  is the mean free path for elastic scattering and  $l_e$  for inelastic scattering. The latter loses momentum after collisions with impurities and the vibrating atomic lattice. These traditional requirements restrict the materials, temperatures and systems where viscous electron flow can be reached<sup>7</sup>. Hence, less restrictive routes<sup>3</sup> towards viscous flow, such as the recently discovered para-hydrodynamics<sup>9,15</sup>, are desirable since they would facilitate the development of new applications such as less energy-demanding devices.

The aim of this work is to rigorously explore the requirements for collective behavior of the electrons. By solving the Boltzmann transport equation (BTE), which is assumed to be exact as described in Supplementary Note 1, the electron distribution is obtained. Transport may be collective or not, depending on the particular magnitude of the length scales  $W$ ,  $l_e$ ,  $l_{ee}$ , and eventually, the cyclotron radius  $l_B$  due to a magnetic field and a length scale  $l_\omega$  associated to an ac driving, as well as on the edge scattering properties.

When the electronic behavior is collective<sup>12,16,17</sup>, the NSE gives correct predictions for macroscopic variables such as the drift velocity. It is worth

mentioning that although the formal derivation of the NSE in conventional fluids is based on the conservation of the number of particles, the momentum and the energy of the fluid, in solid-state systems, the unavoidable electron interaction with phonons and defects implies that the total momentum is not conserved. The latter is usually considered by including a dissipative term in a modified condensed-matter NSE<sup>1,2,7,13</sup>. As a consequence such term extends the validity of this modified NSE to account for the diffusive regime of transport, that cannot be considered as hydrodynamics. In this regime the considered NSE and the well-known Drude model (DRE) give rise to the same results. In our work we propose the accuracy of the NSE and the DRE, which are assessed by comparison with the BTE results, as a fundamental and quantitative criterion for viscous electron flow. Collective behavior is associated with accurate NSE predictions but unaccurate DRE predictions, as otherwise it would be diffusive. Moreover, it is robust regardless of choosing the total current, the velocity or the Hall profile as the observable of interest. In this paper, we study the requirements for viscous electron flow in terms of the characteristic physical length scales and we discuss how the alternative routes affect the most remarkable hydrodynamic signatures above mentioned.

## Results

### Boltzmann transport equation

Consider a 2D system where electrons behave as semiclassical particles<sup>18,19</sup>, with a well-defined position vector  $\mathbf{r} = (x, y)$  and wave vector  $\mathbf{k} = (k_x, k_y)$ , and let  $\hat{f}(\mathbf{r}, \mathbf{k}, t)$  be their distribution function that obeys the BTE<sup>19–22</sup>

$$\partial_t \hat{f} + \mathbf{v} \cdot \nabla_{\mathbf{r}} \hat{f} - \frac{e}{\hbar} (-\nabla \hat{V} + \mathbf{v} \times \mathbf{B}) \cdot \nabla_{\mathbf{k}} \hat{f} = \Gamma[\hat{f}], \quad (1)$$

where  $\mathbf{v} = \hbar\mathbf{k}/m$  and  $-e$  are the electron's velocity and charge, respectively,  $\hbar$  the reduced Plank constant and  $m$  the effective mass. Electrons experience a Lorentz force due to a time-harmonic electric potential  $\hat{V}(\mathbf{r}, t) = V(\mathbf{r})e^{i\omega t}$ , either set at the contacts or with an electromagnetic wave of frequency  $\omega$ , and a perpendicular magnetic field  $\mathbf{B} = B\hat{z}$ .  $\Gamma[f]$  is the collision operator, including all sources of electron scattering. Under Callaway's ansatz<sup>23–25</sup>, the collision term splits as  $\Gamma[\hat{f}] = -(\hat{f} - \hat{f}^e)/\tau_e - (\hat{f} - \hat{f}^{ee})/\tau_{ee}$ , where  $\tau_e$  is the relaxation time for inelastic collisions with impurities and phonons towards the equilibrium distribution  $\hat{f}^e$ , and  $\tau_{ee}$  accounts for elastic collisions with other electrons towards the local distribution  $\hat{f}^{ee}$  shifted by the electron drift velocity. The latter may also describe the effect of the para-hydrodynamics<sup>15</sup>. The intermediate tomographic regime<sup>26,27</sup> does not obey Callaway's ansatz, but it may be described assuming two different values for the relaxation rate  $\tau_{ee}$  (see Supplementary Note 2).

We assume the electron density  $n$  to be constant and set by a gate potential, so that  $\hat{f}^e$  does not depend on  $\mathbf{r}$  or  $t$ . Let  $k_F$  be the Fermi wave-number and  $v_F = \hbar k_F/m$  the Fermi velocity in an isotropic band structure. We rewrite  $\mathbf{k} = k\hat{\mathbf{u}}_k$ , with  $\hat{\mathbf{u}}_k \equiv (\cos\theta, \sin\theta)$ , and define  $\hat{g}(\mathbf{r}, \theta, t) \equiv (4\pi^2\hbar/m) \int_0^\infty (\hat{f} - \hat{f}^e) dk$  and  $\hat{g}^{ee}(\mathbf{r}, \theta, t) \equiv (4\pi^2\hbar/m) \int_0^\infty (\hat{f}^{ee} - \hat{f}^e) dk$ . Moreover  $\int_0^{2\pi} \hat{g}(\mathbf{r}, \theta, t) d\theta = 0$  and we assume  $|\hat{g}| \ll v_F$ , namely, phenomena happen near the Fermi surface. We integrate Eq. (1) over  $k$  and look for a solution  $\hat{g}(\mathbf{r}, \theta, t) = \Re[g(\mathbf{r}, \theta)e^{i\omega t}]$ , where  $\Re$  stands for the real part. The following equation holds for the length scales defined in Table 1

$$i \frac{g}{l_\omega} + \hat{\mathbf{u}}_k \cdot \nabla_r \left( g - \frac{eV}{mV_F} \right) + \frac{\partial_\theta g}{l_B} + \frac{g}{l_e} + \frac{g - g^{ee}}{l_{ee}} = 0, \quad (2)$$

where  $g^{ee} \simeq u_x \cos\theta + u_y \sin\theta$  and the components of the drift velocity are  $u_x(\mathbf{r}) = (1/\pi) \int_0^{2\pi} g(\mathbf{r}, \theta) \cos\theta d\theta$  and  $u_y(\mathbf{r}) = (1/\pi) \int_0^{2\pi} g(\mathbf{r}, \theta) \sin\theta d\theta$ .

Previous works have proposed a formalism based on non-local conductivity tensors to solve the BTE and particularly to analyze the hydrodynamic regime<sup>15,28</sup>. However, although formally such approach can be used in arbitrary geometries, its practical application has been reduced so far to limited edges conditions. In this regard, our current proposal overpasses this limitation.

### The Navier–Stokes equation

Let us ignore higher modes of  $g(\theta)$  to find a model equation based on macroscopic variables, this is, the drift velocity  $(u_x, u_y)$  and  $(w_x, w_y)$  which is related to the stress tensor in classical hydrodynamics. We write  $g$  as a distribution depending on these variables<sup>20</sup>

$$g = u_x \cos\theta + u_y \sin\theta + w_x \cos 2\theta + w_y \sin 2\theta. \quad (3)$$

By considering this level of approximation and following the procedure detailed in Supplementary Note 3, Eq. (2) can be recast as

$$\nabla \cdot \mathbf{u} = 0, \quad (4a)$$

$$-\nu \nabla^2 \mathbf{u} + (\omega_B + \nu_H \nabla^2) \mathbf{u} \times \hat{\mathbf{z}} + \left( \frac{v_F}{l_e} + i\omega \right) \mathbf{u} = \frac{e}{m} \nabla V, \quad (4b)$$

that resemble the continuity equation and the NSE for classical fluids<sup>12,7,13</sup>. We define the cyclotron frequency  $\omega_B \equiv eB/m$ , the viscosity  $\nu$  and Hall viscosity  $\nu_H$  as follows<sup>29,30</sup>

$$\nu \equiv \frac{v_F(l_e^{-1} + l_{ee}^{-1} + i\omega^{-1})}{4(l_e^{-1} + l_{ee}^{-1} + i\omega^{-1})^2 + 16l_B^{-2}}, \nu_H \equiv \frac{v_F l_B^{-1}}{2(l_e^{-1} + l_{ee}^{-1} + i\omega^{-1})^2 + 8l_B^{-2}}. \quad (5)$$

We notice that these definitions take into account the contribution of all considered effects, such as those derived from inelastic collisions. Including  $l_e$  in this expression is not new<sup>25</sup> and it is similar to the effects considered by the ballistic correction proposed in previous works<sup>6,13,22</sup>. However in the current proposal it is not a phenomenological correction but

**Table 1 | Length scales in the BTE (2)**

Length scales		
Length	Expression	Name
$l_e$	$v_F \tau_e$	Inelastic mean free path
$l_{ee}$	$v_F \tau_{ee}$	Elastic mean free path
$l_B$	$m v_F / eB = v_F / \omega_B$	Cyclotron radius
$l_\omega$	$v_F / \omega$	ac length

remarkably it arises naturally from our model. Notice that Eq. (4b) has a dissipative term in  $\mathbf{u}$  arising from non-conserving-momentum collisions ( $l_e < \infty$ ), and this is why it contains the Drude equation (DRE) as a particular case.

### Sample boundaries

Boundary conditions that account for edge scattering are crucial to properly describe viscous electron flow within any model<sup>31</sup>. It is generally admitted that a direct comparison between the NSE and the BTE approaches is clearly not trivial. The main difficulty is how to deal with boundary conditions in such a way that both methods could treat the same transport regimes. In the present work, one of the most relevant and innovative achievements is the development of a well-defined formalism to deal with the same edge scattering properties within both models, see Supplementary Note 4. Since the particular boundary details strongly depend on the experimental conditions, we shall study the most currently accepted types of boundary conditions derived from microscopical considerations. First, we consider a fully diffusive (DF) edge where incident electrons are scattered in all directions regardless of their angle of incidence<sup>3</sup>. Second, we analyze a partially specular (PS) edge where scattering is due to the irregularities of the boundary. Notice that this scenario is affected by the boundary roughness defined by way of its dispersion coefficient  $d \equiv \sqrt{\pi} h^2 h' k_F^3 \lesssim 1$ , where  $h$  is the edge's bumps mean height and  $h'$  is its correlation length. The exact expressions for the BTE and the derivation of the NSE conditions in terms of the so-called slip length  $\xi$ <sup>31</sup> are reported in Supplementary Note 4 and result in the following definitions

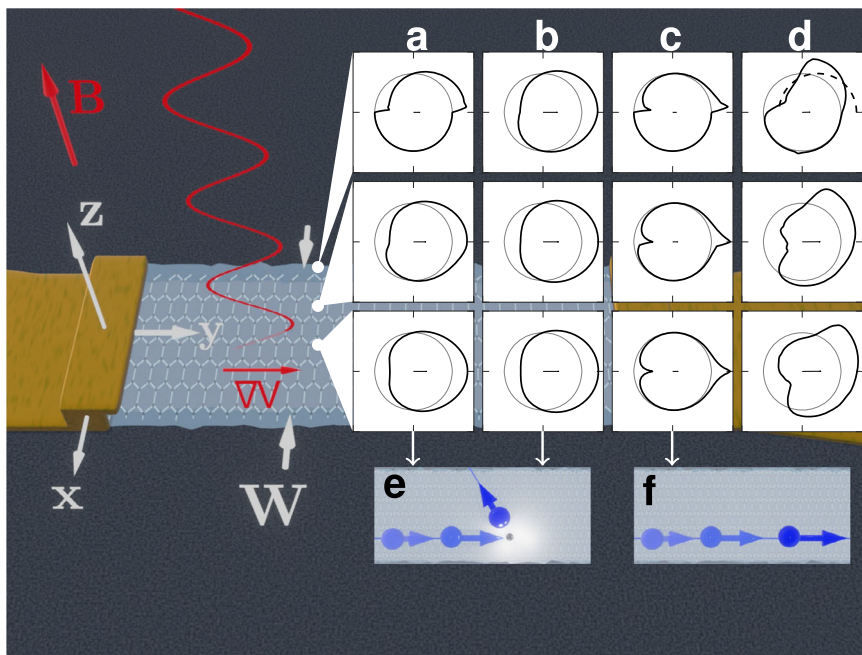
$$\xi = \begin{cases} \frac{3\pi}{4} \frac{\nu}{v_F}, & \text{DF edge,} \\ 8 \left( \frac{1}{d} - \frac{2}{3\pi} \right) \frac{\nu}{v_F}, & \text{PS edge.} \end{cases} \quad (6)$$

Notice that the validity condition  $d \lesssim 1$  prevents the occurrence of negative values of the slip length. These results are compatible with previous studies where the effect of inelastic collisions, magnetic and ac electric fields were neglected<sup>31</sup>. Here, a flat PS edge ( $d=0$ ) leads to the perfect slip boundary condition  $\xi \rightarrow \infty$ , while the no-slip condition  $\xi=0$  remains beyond the microscopic approach.

### Flow in a channel

Figure 1 shows the distribution  $g(\theta)$  given by the BTE for three different positions inside a very long channel under a constant potential gradient  $\partial_y V$ . Let us start discussing the role of the boundary conditions in an intermediate regime transport such that  $l_e = l_{ee} = W$ ,  $l_B$  and  $l_\omega \rightarrow \infty$ . Figure 1a shows the distributions for a DF edge [see Supplementary Eq. (S.6) in the SI] where electrons are uniformly scattered in all directions, while Fig. 1b corresponds to a PS edge [see Supplementary Eq. (S.12) in the SI]. The angular distribution at the edge is less sharp when there is some specularity. Hence, regarding the truncated harmonic expansion (3), we expect the NSE to be more accurate for PS edges than for DF edges. Concerning the ballistic regime ( $l_e = l_{ee} = 10W$ ), Fig. 1c and d present  $g(\theta)$  in absence ( $l_B \rightarrow \infty$ ) and in the presence of a commensurable magnetic field ( $l_B = W$ ), respectively. Although some electrons collide against the walls in the first case, others travel almost parallel to the channel without collisions and continuously increase their momentum. Such an accumulation of electrons traveling

**Fig. 1 | Sketch of a long graphene ribbon and electron flow distributions.** Electrons flow under the effect of a potential gradient  $\nabla V$  and a magnetic field  $\mathbf{B} = B\hat{z}$ . Panels **a–d** show polar plots of the distribution  $g(\theta)$  derived from the Boltzmann transport equation (BTE) for three different positions  $x = 0, -W/4$  and  $-W/2$ , where  $W$  is the width of the channel. Deviations between  $g(\theta)$  and the equilibrium distribution (gray circle) has been enlarged for clarity. **a** Intermediate regime where  $l_e = l_{ee} = W, l_B, l_w \rightarrow \infty$  and a DF edge. **b** Same parameters as in panel **a** but for a PS edge with  $d = 0.5$ . **c** Ballistic regime where  $l_e = l_{ee} = 10W$  and  $l_B, l_w \rightarrow \infty$ . **d** Commensurability effect where  $l_e = l_{ee} = 10W, l_B = W, l_w \rightarrow \infty$  and a DF edge. Notice the lack of incident electrons at the edge in some directions in comparison with the dashed line. Panels **e** and **f** show a schematic representation of the electron velocity for the situations considered in panels **a, b** and **c** respectively. Electron scattering in **e** makes the NSE works properly. Ballistic electrons move parallel to the channel with increasing momentum, as depicted in panel **f**. Supplementary Note 5 presents polar plots of the distribution  $g(\theta)$  for an enlarged set of parameters.



parallel to the channel, depicted in Fig. 1f, accounts for the sharp peak that appears in the pseudo-Fermi distribution in Fig. 1c. The NSE level of approximation based on the consideration of the first two angular harmonics Eq. (3) is clearly not compatible with such  $g(\theta)$ . Conversely, elastic and inelastic collisions keep these electrons from gaining momentum, as depicted in Fig. 1e. Moreover, they relax the angular distribution to smoother functions, as presented in Fig. 1a and b, and make the NSE accurate when  $l_e < W$  or  $l_{ee} < W$ . Interestingly, this is not the case in the so-called tomographic regime<sup>26,27</sup>, as shown in Supplementary Note 2. This regime, which is often considered between the ballistic and hydrodynamic regimes<sup>26,27</sup>, is not fully hydrodynamic according to this criterion.

### Inelastic and elastic collisions

As shown in previous works<sup>5,20</sup>, the curvature of the current density profile in a uniform channel might not be a good indicator for hydrodynamic behavior. However, our approach can be tested in such a physical scenario, as well as in other non-uniform geometries, to evaluate the deviation between the results from the NSE and the BTE instead. Figure 2 shows the velocity profiles for different values of the length scales of the system. Figure 2a accounts for a uniform channel and Fig. 2b for a crenellated one. The main conclusion of Fig. 2 is that the NSE and the BTE predictions are completely different in the ballistic regime, but they almost overlap in the Poiseuille, diffusive, magnetic and ac field panels.

Additionally our results allow us to also understand how all the considered effects result in curved profiles. A Poiseuille profile, which is almost parabolic, emerges when  $l_{ee} \ll W \ll l_e$ , as depicted in Fig. 2c. Nevertheless, a nonzero curvature of the velocity profile is not unique to this regime. Even in the diffusive regime  $l_e \ll W$  shown in Fig. 2d, and in the absence of elastic collisions  $l_{ee} \gg W$ , the profile is not flat. Figure 2e shows the ballistic regime for comparison.

Figure 2f and g proves the hydrodynamic behavior and curvature in presence of a magnetic field and an ac field respectively. Although previously suggested<sup>32</sup>, we prove that the former is a stronger hydrodynamic fingerprint by a direct comparison between the BTE and the NSE. Most remarkably, the hydrodynamic features can also be induced by the application of an ac field. For completeness, Supplementary Note 6 shows the prediction of the velocity profile in an extended set of transport regimes, where in addition the DRE solution is shown as a wrong approximation to

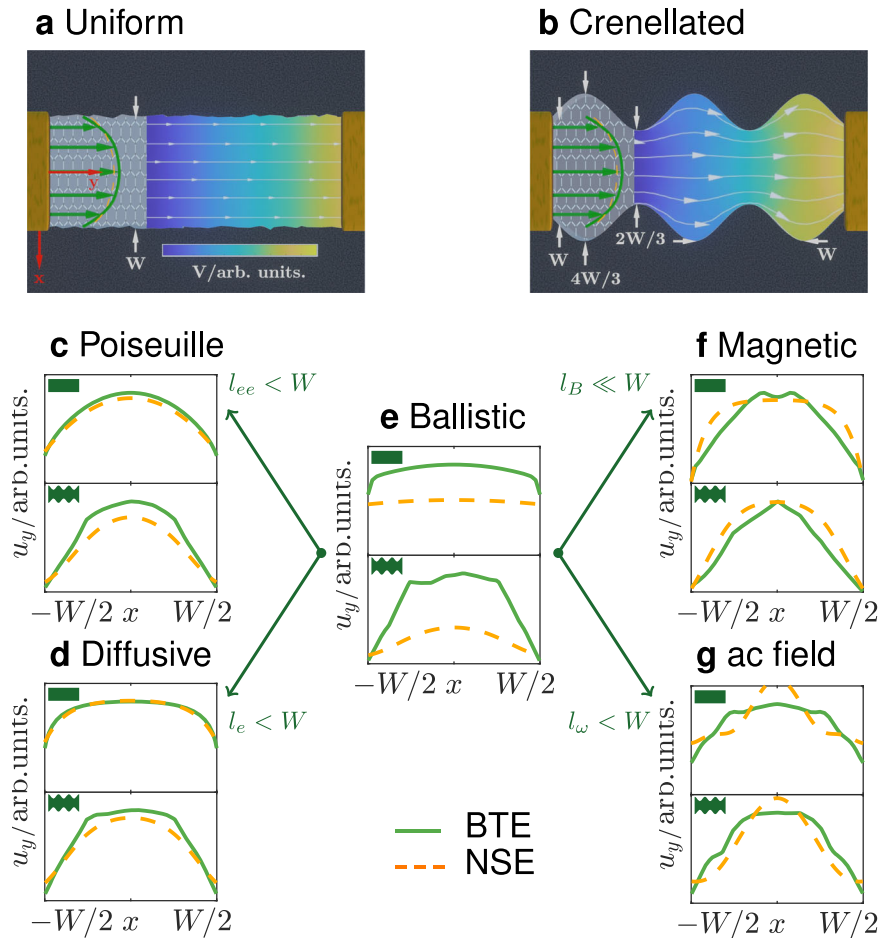
the problem. A detailed derivation of the DRE is presented in Supplementary Note 7.

### Magnetic and AC fields

Let us now focus on the deviations of the NSE predictions from the BTE results. To this end, we calculate the electric current  $I_{NSE}$  and  $I_{BTE}$  from the velocity profile obtained after solving the NSE and the BTE, respectively, and define the relative error as  $\epsilon = 2|I_{NSE} - I_{BTE}| / |I_{NSE} + I_{BTE}|$ , as explained in Methods. The electric current is proportional to the area under each velocity profile, and it is a relevant quantity in most experiments<sup>5,33,34</sup>. The accuracy of the DRE has been accounted accordingly in Supplementary Note 8 to monitor the parameters that lead to identical results of the BTE, NSE and DRE, namely, the diffusive regime of transport.

Figure 3a shows the NSE error when compared to the BTE in the presence of a magnetic field and considering different boundary conditions. Notice that the gray patterned area corresponds to the conventional requirements for hydrodynamic onset. The red contour line limits the region where the NSE error is larger than 20%, defined as the ballistic regime of transport. Similarly the blue contour line surrounds the diffusive regime (blue area) such as the DRE error is smaller than 20%. We remark that these results would be similar if we choose a threshold within 10% and 30% to define the different transport regimes. Thus, white regions account for reliable sets of parameters supporting hydrodynamic transport. In all considered cases, our results demonstrate the validity of the NSE beyond the usually accepted conditions (see white areas). Indeed, the increase of the magnetic field also benefits the hydrodynamic regime as demonstrated in Fig. 3a. Still, the region of validity slightly shrinks for the particular case  $l_B \approx W$ . The latter occurs due to the already known commensurability effect of resistance<sup>35</sup>, that some works referred to as a phase transition<sup>32</sup>. In this particular situation, cyclotron orbits prevent electrons coming from a particular edge to reach the opposite one with all angles, as shown in Fig. 3c. Furthermore, Fig. 1d proves that this effect depletes entire regions of the pseudo-Fermi distribution, and Supplementary Eq. (S.7) for the incident distribution at the wall fails. Therefore, as a general trend, increasing the magnetic field while keeping  $l_B \approx W$  makes the NSE valid, as shown in Fig. 3a. Still there is a field threshold above which the system will eventually enter the diffusive regime of transport. Indeed, a Lorentz force, not balanced by a Hall field, prevents electrons from following straight trajectories, as illustrated in Fig. 3d.

**Fig. 2 | Electron flow simulations in a very long uniform channel and a crenellated one with diffusive (DF) boundaries.** Panels **a** and **b** show the Boltzmann transport equation (BTE) potentials and electron streamlines in the Poiseuille regime. **c** Profiles of the drift velocity along the channel with frequent elastic collisions ( $l_{ee} = 0.25W$ ) is the usual route to viscous electron flow and result in a Poiseuille flow. **d** Profiles with frequent inelastic collisions ( $l_e = 0.25W$ ) is the usual route to viscous electron flow and result in a Poiseuille flow. **e** Ballistic regime where the Navier–Stokes equation (NSE) results in wrong predictions. Here  $l_e = l_{ee} = 10W$  for the uniform channel and  $l_e = l_{ee} = 2W$  for the crenellated one. In the latter the uneven walls have an stronger effect on the electron flow and thus it presents ballistic behavior even for slightly shorter  $l_e$  and  $l_{ee}$ . **f** Profiles in the presence of a magnetic field ( $l_B = 0.25W$ ). **g** Profiles in the presence of an ac field ( $l_\omega = 0.25W$ ). This figure shows the accuracy of the NSE to reproduce the curved velocity profile.



We also study the effects of an ac electric field polarized along the channel when a magnetic field is also applied. Then there is an overall decrease in the NSE’s error when  $l_e \gg W$  and  $l_{ee} \gg W$ , shown in Fig. 3b. If we consider electrons traveling parallel to the channel, while they are increasing momentum the ac field swaps its direction leading to slow them down, as shown in Fig. 3e. Thus, inertia avoids the formation of peaks such as those highlighted in Fig. 1c and makes the NSE valid under an ac field, as also demonstrated in Fig. 3b. However, we find an increase in the error due to the cyclotron resonance condition  $l_B \simeq l_\omega$  ( $\omega_B \simeq \omega$ ), so that both effects couple and mutually hinder, as depicted in Fig. 3f. Figure 3 also sheds light on the transition from the diffusive to the ballistic regime when changing the various length scales involved in charge transport. It is apparent from Fig. 3 that, in almost all cases studied, the transition is not abrupt but an intermediate transport regime is reached, where the NSE describes accurately non-equilibrium collective electron dynamics (see white areas).

It is worth noticing that some authors suggest the Hall field instead of the current density profile to assess the hydrodynamic regime<sup>5,20</sup>. However, from this perspective, the consideration of the current profiles, the Hall voltage, the total current or the total Hall voltage yields the same conclusions, as proven in Supplementary Note 10.

In summary, according to the analysis of the transverse velocity profiles (see Fig. 2) and the evaluated error of the NSE in comparison with the BTE (see Fig. 3), we demonstrate that the traditional requirement for hydrodynamic transport in solid-state systems,  $l_{ee} < W$ , can be overcome by the alternative routes whose general trends are summarized in Fig. 3: i) keep the inelastic scattering length within the order of the device size,  $l_e \sim W$ , ii) include a magnetic field such that a  $l_B$  is the same order of magnitude as  $W$  but different from the commensurability condition and iii) the application of an ac field such that a  $l_\omega \sim W$ .

Error maps shown in Fig. 3a also include typical physical conditions considered in some experiments for comparison<sup>6,13,36</sup>. Supplementary Note 9 reports on the detailed description of the considered sets of parameters. Notice that although some materials, such as low quality graphene  $G_{SiO_2}$ , never enter the conventionally accepted region,  $G_{SiO_2}$  narrow channels may enter the hydrodynamic regime by way of the alternative routes. Our analysis changes the widely accepted paradigm and proves that more materials and more temperatures can be studied using hydrodynamics tools. This also establishes that the ratio  $l_{ee}/l_e$  is not so crucial concerning the validity of the NSE. As a reference, let us remark that for a graphene ribbon of width  $W = 500$  nm at  $n = 10^{12}$  electrons/cm<sup>2</sup>,  $l_B = 500$  nm ( $B \simeq 250$  mT), while  $l_\omega = 500$  nm ( $\omega/2\pi \simeq 0.3$  THz), so both  $l_B \sim W$  and  $l_\omega \sim W$ , are plausible requirements.

### Discussion

The hydrodynamic routes proposed in this work shed light on some of generally admitted signatures of viscous electron flow. Let us focus first on non-local experiments based on uniform Hall bars in the so-called proximity geometry<sup>6–8</sup>. The existence of a transition from ballistic to hydrodynamic transport regimes has been demonstrated based on the occurrence of a sharp maximum in the negative resistance<sup>8</sup>. Notice that this effect is also related to the existence of unexpected backflow or even small whirlpools due to the viscous nature of the electron flow. The conventional hydrodynamic description, which requests the condition  $l_{ee} < W$ , agrees with their measurements at intermediate temperatures. However, the fact that the hydrodynamic onset survives at very low temperatures when  $l_{ee} \rightarrow \infty$ , is incompatible with  $l_{ee} < W$ . Remarkably, the latter is indeed compatible with our results, since we have demonstrated that the condition  $l_e \sim W$  is already sufficient for the hydrodynamic transport to occur (Supplementary

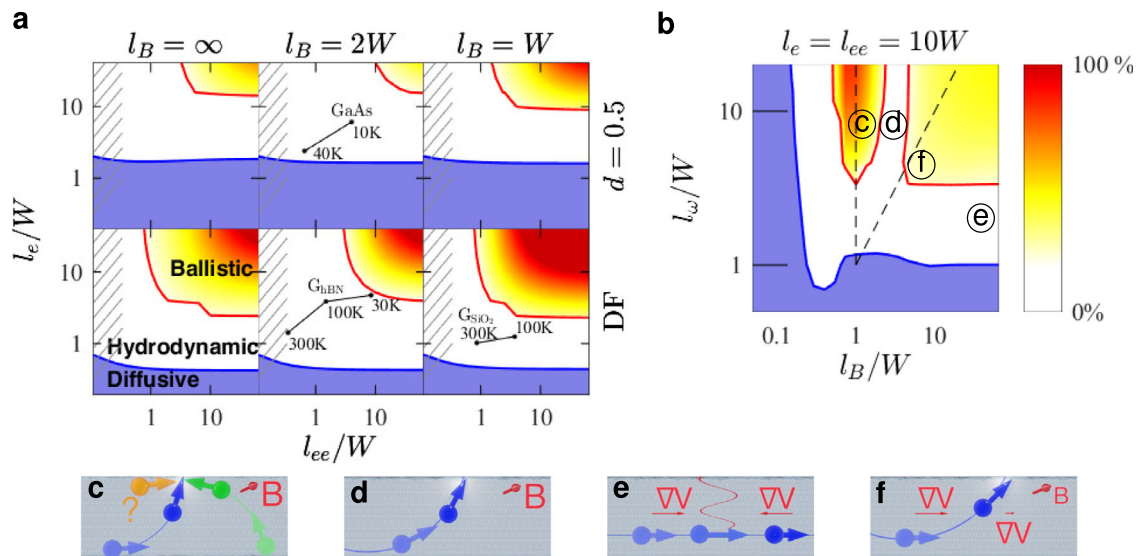


**Fig. 3 | Error of the total current obtained with the Navier–Stokes equation (NSE) in comparison with the Boltzmann transport equation (BTE) results.** White regions remark the hydrodynamic regime where only NSE results are correct and blue regions are those where both the NSE and the Drude equation (DRE) account for the diffusive regime of transport. Red (blue) contour lines limit the region where the NSE (DRE) error is 20%. **a** NSE error versus  $l_e$  and  $l_{ee}$  mean free paths, in absence of an ac field. Each plot accounts for a DF or PS ( $d = 0.5$ ) edge, and for a different cyclotron radius. Gray patterned areas, defined by the conditions  $l_{ee} < W/3$  and  $l_e < l_e/3$ , indicate the conventional requirements ( $l_{ee} \ll W$  and  $l_e \ll l_e$ ) to achieve the hydrodynamic regime. For comparison, overprinted lines show typical physical conditions considered in some experiments in high quality graphene ( $G_{hBN}$ ) in a  $W = 500$  nm-wide channel<sup>6,36</sup>, graphene on a  $SiO_2$  substrate ( $G_{SiO_2}$ )<sup>42</sup> and GaAs ( $G_{As}$ )<sup>13</sup> in a  $W = 200$  nm-wide channel (see Supplementary Note 9). **b** NSE error

versus the cyclotron radius  $l_B$  and the ac length  $l_\omega$  for  $l_e = l_{ee} = 10W$  and a DF edge. Commensurability resistance happens when  $l_B \approx W$  and cyclotron resonance when  $l_B \approx l_\omega$ . Panels c–f represent electrons as semiclassical particles moving under a potential gradient  $\nabla V$  and a perpendicular magnetic field  $B$ , for some relevant positions labeled in panel b. **c** Commensurability effect arises when electrons cannot reach the boundaries in all directions. **d** Electrons do not follow straight trajectories under a magnetic field. **e** An electron moving parallel to the channel and subject to an ac electric field will alternately accelerate and decelerate due to the field swiping direction. **f** The magnetic field and the ac electric field mutually hinder when  $l_\omega = l_B$ , namely the resonant condition  $\omega = \omega_B$  is met. Supplementary Note 8 shows error maps evaluated by means of the total electric current for an enlarged set of parameters.

Note 12). The fact that the hydrodynamic regime only exists at low carrier density is consistent with  $l_e$  decreasing near the neutrality point<sup>7</sup>.

The alternative route  $l_e \sim W$  is also supported by the direct visualization of the Poiseuille flow of an electron fluid<sup>5</sup>. Here, the Hall field profile across a high-mobility graphene channel is used as the key for distinguishing ballistic from hydrodynamic flow. A curved profile is not unique to the conventional situation  $l_{ee} < W$ , as it also arises when  $l_e \sim W$ , in agreement with Fig. 2c. Within the same experimental setup, another alternative route with the magnetic field is made clear. Indeed, the authors find a sharp increase in the profile curvature when increasing the magnetic field, showing that our proposed condition to tune  $l_B$  triggers the hydrodynamic onset of the NSE.

Last let us comment on the experimental hydrodynamic evidence known as superballistic conduction. This regime of collective transport refers to devices with a resistance under its ballistic limit<sup>6,13,22</sup>. We notice the superballistic regime cannot be exclusively related to the case of frequent elastic collisions, since it can also be reached with the proposed alternative routes as shown in Supplementary Fig. 8. Particularly under the condition  $l_B \ll W$ , such phenomenon is known as negative magnetoresistance<sup>13,29</sup>. Other experiments<sup>35</sup> show how, after the resistance peak due to the commensurability effect ( $l_B = W$ ), a further increase of the magnetic field  $l_B \ll W$  results in a resistance under the ballistic limit.

### Conclusion

To conclude, in this work we develop a framework to approximate the general BTE to the simplified NSE and to define where electron transport is hydrodynamic. We believe that our approach has several advantages, mainly because it is rigorously based on the requirements for collective behavior as a fundamental premise. This allows us to perform our analysis with no need of initial assumptions for the viscosity, so that its dependence on all length scales ( $l_e, l_{ee}, l_B, l_\omega, W$ ) arises naturally. In addition, our approach is not directly related to geometrical constraints so it can be

applied in many other physical scenarios. We conclude that the widely admitted requirements for viscous electron flow are too restrictive and limit hydrodynamic transport to very particular experimental conditions, regarding temperature range or materials quality. Remarkably, the alternative routes actually lead to the most noteworthy hydrodynamic signatures. Our proposal to search for hydrodynamic signatures for ac electric fields<sup>11,21</sup> is still an open question in experiments. Although the generally admitted route  $l_{ee} < W$ , combined with  $l_e < l_e$ , is the easiest situation where hydrodynamic flow can be decoupled from other effects, finding materials with high  $l_e/l_{ee}$  ratios is a major issue<sup>1,2,37</sup>. Thus, the relevance of the alternative routes, compatible with viscous flow, greatly expands the possible scenarios where traditional hydrodynamic features may occur or even unexpected phenomena may arise.

### Methods

The BTE is solved using a finite element method<sup>38</sup>. Unlike the nonlocal conductivity formalism<sup>15,28</sup>, it can be implemented for arbitrary boundary conditions. In a very long channel, the electric potential splits as  $V(x, y) = V_H(x) + y\partial_y V$ , where  $V_H(x)$  is the Hall potential and  $\partial_y V$  is a constant potential gradient. Therefore,  $g = g(x, \theta)$  does not depend on  $y$  and the BTE (2) reduces to

$$i \frac{g}{l_\omega} + \cos \theta \partial_x \left( g - \frac{eV}{mv_F} \right) + \sin \theta \partial_y V + \frac{\partial_\theta g}{l_B} + \frac{g}{l_e} + \frac{g - g^{ee}}{l_{ee}} = 0. \quad (9)$$

We approximate the potential  $V_H$  by its expansion in a truncated basis  $\{\phi_n(x)\}_{n=1}^N$  of tent functions defined on  $[-W/2, W/2]$  as  $V_H(x) =$

$\sum_{n=1}^N V_n \phi_n(x)$  and write the solution as

$$g(x, \theta) = \sum_{n=1}^N \sum_{m=1}^M g_{nm} \phi_n(x) \varphi_m(\theta), \quad (8)$$

where  $\{\varphi_m(\theta)\}_{m=1}^M$  is a periodic basis of tent functions defined on  $[0, 2\pi)$ . We achieved convergence for  $N \gtrsim 40$  and  $M \gtrsim 32$ . We found the weak form of Eq. (2) and used a conforming Galerkin method to write the  $N \times M$  system of linear equations. The resulting system is sparse in the spatial part and includes the boundary conditions for the scattered electrons. No-trespassing condition ( $u_x = 0$ ) is enforced, unless within a magnetic field, where the solution was later corrected to ensure no-trespassing condition. For 2D arbitrary geometries, the same procedure is applied to Eq. (2). We set the  $g(\theta)$  distribution at the contacts, far away from the studied region, using as an input the result for simulations in uniform channels. We rewrite the equations at all other edges for the corresponding boundary conditions. We use  $N \sim 10^4$  spatial elements for arbitrary geometries, with a triangle size  $\leq 0.2W$  and an adaptive method with a thinner meshing near the corners, and a smaller  $M \sim 16$  to reduce computational cost.

The NSE was solved analytically in a very long channel (see Supplementary Section 11 of the SI) and numerically in other geometries using the finite element method<sup>39</sup>, with triangular<sup>40</sup> Taylor-Hood elements<sup>41</sup>. We imposed mixed boundary conditions<sup>31</sup>, used the analytical solution in a channel to set the velocities at the contacts and imposed a constant potential and zero current flow at the metallic contacts. The fourth-order Runge-Kutta method was used to compute the streamlines. The NSE and DRE errors are defined comparing to the BTE results as  $\varepsilon \equiv 2|I_{\text{NSE}} - I_{\text{BTE}}| / |I_{\text{NSE}} + I_{\text{BTE}}|$  and  $\varepsilon_{\text{DR}} \equiv 2|I_{\text{DRE}} - I_{\text{BTE}}| / |I_{\text{DRE}} + I_{\text{BTE}}|$  where  $I = -en \int_{-W/2}^{W/2} u_y dx$  is the total current, proportional to the area under the velocity profile. In order to identify the diffusive regions, the quantity  $1 - \varepsilon_{\text{DR}}$  indicates where the DRE equation is correct.

## Data availability

The data supporting the findings of this study are available from the corresponding author upon request.

## Code availability

The computer code supporting the findings of this study is available from the corresponding author upon request.

Received: 8 February 2024; Accepted: 16 April 2024;

Published online: 29 April 2024

## References

- Polini, M. & Geim, A. K. Viscous electron fluids. *Phys. Today* **73**, 28 (2020).
- Narozhny, B. N. Hydrodynamic approach to two-dimensional electron systems. *Riv. Nuovo Cimento* **45**, 1 (2022).
- Fritz, L. & Scaffidi, T. Hydrodynamic electronic transport. *Ann. Rev. Condensed Matter Phys.* **15**, 17–44 (2024).
- Varnavides, G., Yacoby, A., Felser, C. & Narang, P. Charge transport and hydrodynamics in materials. *Nat. Rev. Mater.* **8**, 726 (2023).
- Sulpizio, J. A. et al. Visualizing Poiseuille flow of hydrodynamic electrons. *Nature* **576**, 75 (2019).
- Krishna Kumar, R. et al. Superballistic flow of viscous electron fluid through graphene constrictions. *Nat. Phys.* **13**, 1182 (2017).
- Bandurin, D. et al. Negative local resistance caused by viscous electron backflow in graphene. *Science* **351**, 1055 (2016).
- Bandurin, D. A. et al. Fluidity onset in graphene. *Nat. Commun.* **9**, 4533 (2018).
- Aharon-Steinberg, A. et al. Direct observation of vortices in an electron fluid. *Nature* **607**, 74 (2022).
- Huang, W. et al. Electronic Poiseuille flow in hexagonal boron nitride encapsulated graphene field effect transistors. *Phys. Rev. Res.* **5**, 023075 (2023).
- Farrell, J. H., Grisouard, N. & Scaffidi, T. Terahertz radiation from the Dyakonov-Shur instability of hydrodynamic electrons in Corbino geometry. *Phys. Rev. B* **106**, 195432 (2022).
- Résibois, P. & De Leener, M. *Classical Kinetic Theory of Fluids* (John Wiley & Sons, 1977).
- Keser, A. et al. Geometric control of universal hydrodynamic flow in a two-dimensional electron fluid. *Phys. Rev. X* **11**, 031030 (2021).
- Golse, F. The Boltzmann equation and its hydrodynamic limits. In *Handbook of Differential Equations Evolutionary Equations*, vol. 2 of *Handbook of Differential Equations: Evolutionary Equations*, (eds. Dafermos, C. M. & Feireisl, E.) 159 (North-Holland, 2005).
- Wolf, Y., Aharon-Steinberg, A., Yan, B. & Holder, T. Parahydrodynamics from weak surface scattering in ultraclean thin flakes. *Nat. Commun.* **14**, 2334 (2023).
- Balescu, R. *Equilibrium and nonequilibrium statistical mechanics* (Krieger Publishing Company, 1991).
- Soto, R. *Kinetic theory and transport phenomena*, vol. 25 (Oxford University Press, 2016).
- Ashcroft, N. W. & Mermin, N. D. *Solid State Physics* (Thomson Learning, 1976).
- Di Ventra, M. *Electrical Transport in Nanoscale Systems* (Cambridge University Press, 2008).
- Holder, T. et al. Ballistic and hydrodynamic magnetotransport in narrow channels. *Phys. Rev. B* **100**, 245305 (2019).
- Kapralov, K. & Svintsov, D. Ballistic-to-hydrodynamic transition and collective modes for two-dimensional electron systems in magnetic field. *Phys. Rev. B* **106**, 115415 (2022).
- Guo, H., Ilseven, E., Falkovich, G. & Levitov, L. S. Higher-than-ballistic conduction of viscous electron flows. *Proc. Natl. Acad. Sci. U.S.A.* **114**, 3068 (2017).
- Callaway, J. Model for lattice thermal conductivity at low temperatures. *Phys. Rev.* **113**, 1046 (1959).
- Varnavides, G., Jermyn, A. S., Anikeeva, P. & Narang, P. Probing carrier interactions using electron hydrodynamics. Preprints at <https://arxiv.org/abs/2204.06004> (2022).
- De Jong, M. J. M. & Molenkamp, L. W. Hydrodynamic electron flow in high-mobility wires. *Phys. Rev. B* **51**, 13389 (1995).
- Ledwith, P., Guo, H., Shytov, A. & Levitov, L. Tomographic dynamics and scale-dependent viscosity in 2d electron systems. *Phys. Rev. Lett.* **123**, 116601 (2019).
- Hofmann, J. & Das Sarma, S. Collective modes in interacting two-dimensional tomographic fermi liquids. *Phys. Rev. B* **106**, 205412 (2022).
- Nazaryan, K. G. & Levitov, L. Robustness of vorticity in electron fluids. Preprint at <https://arxiv.org/abs/2111.09878> (2021).
- Alekseev, P. S. Negative magnetoresistance in viscous flow of two-dimensional electrons. *Phys. Rev. Lett.* **117**, 166601 (2016).
- Berdyugin, A. I. et al. Measuring Hall viscosity of graphene's electron fluid. *Science* **364**, 162 (2019).
- Kiselev, E. I. & Schmalian, J. Boundary conditions of viscous electron flow. *Phys. Rev. B* **99**, 035430 (2019).
- Afanasiev, A. N., Alekseev, P. S., Greshnov, A. A. & Semina, M. A. Ballistic-hydrodynamic phase transition in flow of two-dimensional electrons. *Phys. Rev. B* **104**, 195415 (2021).
- Kumar, C. et al. Imaging hydrodynamic electrons flowing without Landauer-Sharvin resistance. *Nature* **609**, 276 (2022).
- Ella, L. et al. Simultaneous voltage and current density imaging of flowing electrons in two dimensions. *Nat. Nanotechnol.* **14**, 480 (2019).
- Masubuchi, S. et al. Boundary scattering in ballistic graphene. *Phys. Rev. Lett.* **109**, 036601 (2012).

36. Castro Neto, A. H., Guinea, F., Peres, N. M. R., Novoselov, K. S. & Geim, A. K. The electronic properties of graphene. *Rev. Mod. Phys.* **81**, 109 (2009).
37. Bernabeu, J. & Cortijo, A. Bounds on phonon-mediated hydrodynamic transport in a type-I Weyl semimetal. *Phys. Rev. B* **107**, 235141 (2023).
38. Guermond, J.-L. A finite element technique for solving first-order PDEs in  $L^p$ . *SIAM J. Numer. Anal.* **42**, 714 (2004).
39. Ciarlet, P. G. *The Finite Element Method for Elliptic Problems* (SIAM, Philadelphia, 2002).
40. Engwirda, D. *Locally optimal delaunay-refinement and optimisation-based mesh generation* (University of Sydney, 2014).
41. Pacheco, D. R. Q. & Steinbach, O. Space-time Taylor-Hood elements for incompressible flows. *Comput. Methods Mater. Sci.* **19**, 64 (2019).
42. Dean, C. R. et al. Boron nitride substrates for high-quality graphene electronics. *Nat. Nanotechnol.* **5**, 722 (2010).

### Acknowledgements

We wish to acknowledge R. Brito, G. Oleaga, A. Cortijo, J. Bernabeu, B. Zhou, E. Diez and M. Amado for discussions. This work was supported by the “(MAD2D-CM)-UCM” project funded by Comunidad de Madrid, by the Recovery, Transformation and Resilience Plan, and by NextGenerationEU from the European Union and Agencia Estatal de Investigación of Spain (Grant PID2022-136285NB-C31). J.E. acknowledges support from the Spanish Ministerio de Ciencia, Innovación y Universidades (Grant FPU22/01039).

### Author contributions

J.E. did the analytical and numerical calculations. J.E., F.D.-A. and E.D. analyzed the results and wrote the manuscript. F.D.-A. and E.D. supervised the project.

### Competing interests

The authors declare no competing interests.

### Additional information

**Supplementary information** The online version contains supplementary material available at <https://doi.org/10.1038/s42005-024-01632-7>.

**Correspondence** and requests for materials should be addressed to Jorge Estrada-Álvarez.

**Peer review information** *Communications Physics* thanks the anonymous reviewers for their contribution to the peer review of this work.

**Reprints and permissions information** is available at <http://www.nature.com/reprints>

**Publisher’s note** Springer Nature remains neutral with regard to jurisdictional claims in published maps and institutional affiliations.

**Open Access** This article is licensed under a Creative Commons Attribution 4.0 International License, which permits use, sharing, adaptation, distribution and reproduction in any medium or format, as long as you give appropriate credit to the original author(s) and the source, provide a link to the Creative Commons licence, and indicate if changes were made. The images or other third party material in this article are included in the article’s Creative Commons licence, unless indicated otherwise in a credit line to the material. If material is not included in the article’s Creative Commons licence and your intended use is not permitted by statutory regulation or exceeds the permitted use, you will need to obtain permission directly from the copyright holder. To view a copy of this licence, visit <http://creativecommons.org/licenses/by/4.0/>.

© The Author(s) 2024